Geophysical Research Letters

Supporting Information for

Significant Effective Radiative Forcing of Stratospheric Wildfire Smoke

Cheng-Cheng Liu[1], Robert W. Portmann[2], Shang Liu[1,3], Karen H. Rosenlof[2], Yifeng Peng,[4] and Pengfei Yu[5]

[1]School of Earth and Space Sciences, University of Science and Technology of China, Hefei, Anhui, China

[2]Chemical Science Laboratory, National Oceanic and Atmospheric Administration, Boulder, CO, USA

[3]Now at: Research Division, California Air Resources Board, Sacramento, CA, USA

[4]College of Atmospheric Sciences, Lanzhou University, Lanzhou, Gansu, China

[5]Institute for Environmental and Climate Research, Jinan University, Guangzhou, Guangdong, China

Correspondence:

Pengfei Yu (pengfei.yu@colorado.edu), Shang Liu (shangliu2012@gmail.com)

Contents of this file

Text S1. Model Configuration and Experiments

We used prescribed sea surface temperature and sea ice concentration (Hurrell et al., 2008). A modified deep convective transport scheme considering aerosol secondary activation was updated in the model (Froyd et al., 2022; Yu et al., 2019a). The emission inventory for pyroCb smoke was based on our previous modeling (Yu et al., 2021; Yu et al., 2019b) and datasets estimated from satellites (Fromm et al., 2010; Peterson et al., 2018; Peterson et al., 2021). We added additional emissions for pyroCb into one model grid for BC and primary organic matter in MAM3. Detailed information on the injected smoke in our model is in Table S1. In the current study, no pyroCb event was simulated between 2018 and 2019 Dec. 28.

The model was configured with a horizontal resolution of 1.9° latitude × 2.5° longitude and a vertical resolution of 56 pressure levels. This vertical level extended from the surface to nearly 45 km, including about 26 levels above the tropopause (about 200 hPa) with a vertical resolution of about 1 km in the upper troposphere and lower stratosphere.

The model was spun up with specified dynamics from 2017 Jan. 1 until 2017 Aug. 12 for the beginning of the PNE event. The dynamics were nudged to the meteorology of the Goddard Earth Observing System Data Assimilation System Version 5 (GEOS5) reanalysis. Subsequently, for the following time until June 2021, we conducted the free-run ensembles with model-generated meteorology.

Text S2. Satellite Observations

The Ozone Mapping and Profiler Suite (OMPS) Limb Profiler (LP) was deployed onboard the Suomi National Polar-orbiting Partnership satellite. The OMPS-LP sampled >7000 vertical profiles each day with global coverage in 3-4 days after January 2012. The aerosol extinction coefficient at 675 nm was retrieved from the radiance measurements for OMPS-LP level 2 version 1 (Loughman et al., 2018), although with a coarser retrieved vertical resolution, the OMPS-LP dataset reported the measured 1-km vertical profiles from about 10 to 40 km.

The Stratospheric Aerosol and Gas Experiment III on the International Space

Station (SAGE III/ISS) measured attenuation of solar radiation by atmospheric constituents after June 2017 (Knepp et al., 2020). SAGE III/ISS observed during sunrise or sunset and measured up to 31 profiles per day (Chen et al., 2020). The total coverage was between 70° N/S, with a higher frequency at midlatitudes. SAGE III/ISS provided aerosol extinction coefficients at 9 wavelengths from 384 to 1543 nm, with a high precision of about 5 % bias for the main aerosol layer (Knepp et al., 2020). The vertical resolution of these data was 0.75 km, reported per 0.5 km from 0 to 45 km. The SAGE III/ISS level 2 solar products version 5.2 was used in this work.

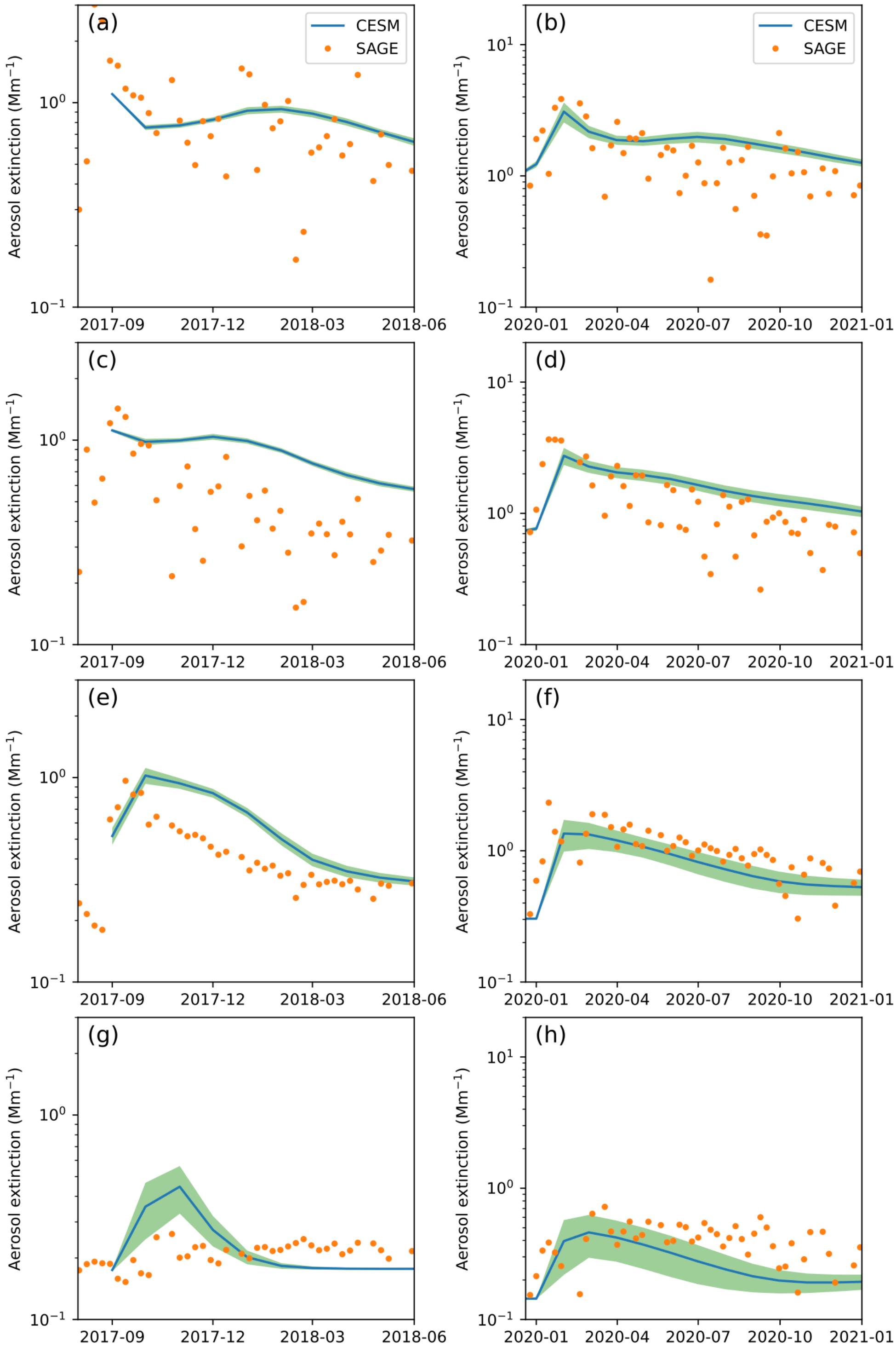

Figure S1. Comparison of the mid-latitude aerosol extinction coefficients for CESM and SAGE III/ISS for 2017 PNE (left) and 2019-2020 ANY (right). The top to bottom panels represent aerosol extinction coefficients at 675 nm for 12-13 km, 15-16 km, 18-19 km, and 21-22 km, respectively. The green shading denotes the standard deviation of the ensembles.

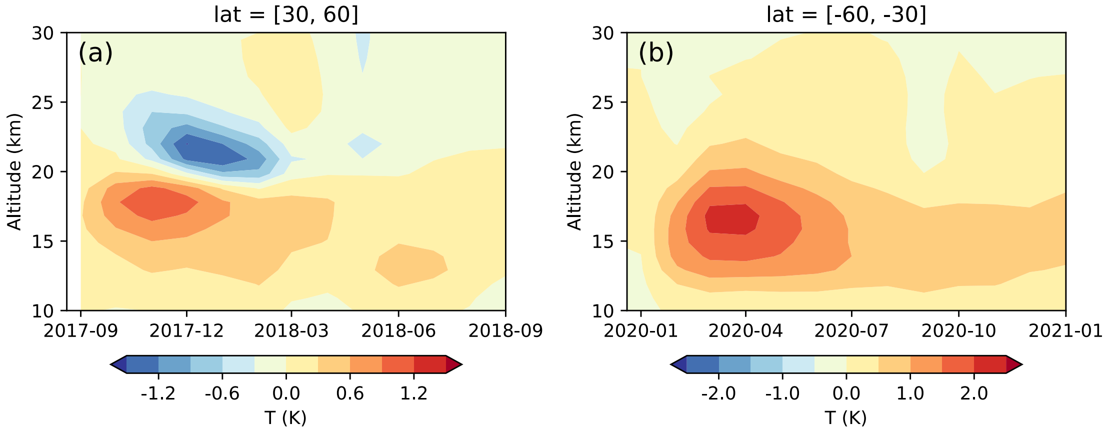

Figure S2. Regional temperature anamaly over the midlatitudes for (a) 2017 PNE in the Northern Hemisphere and (b) 2019-2020 ANY in the Southern Hemisphere.

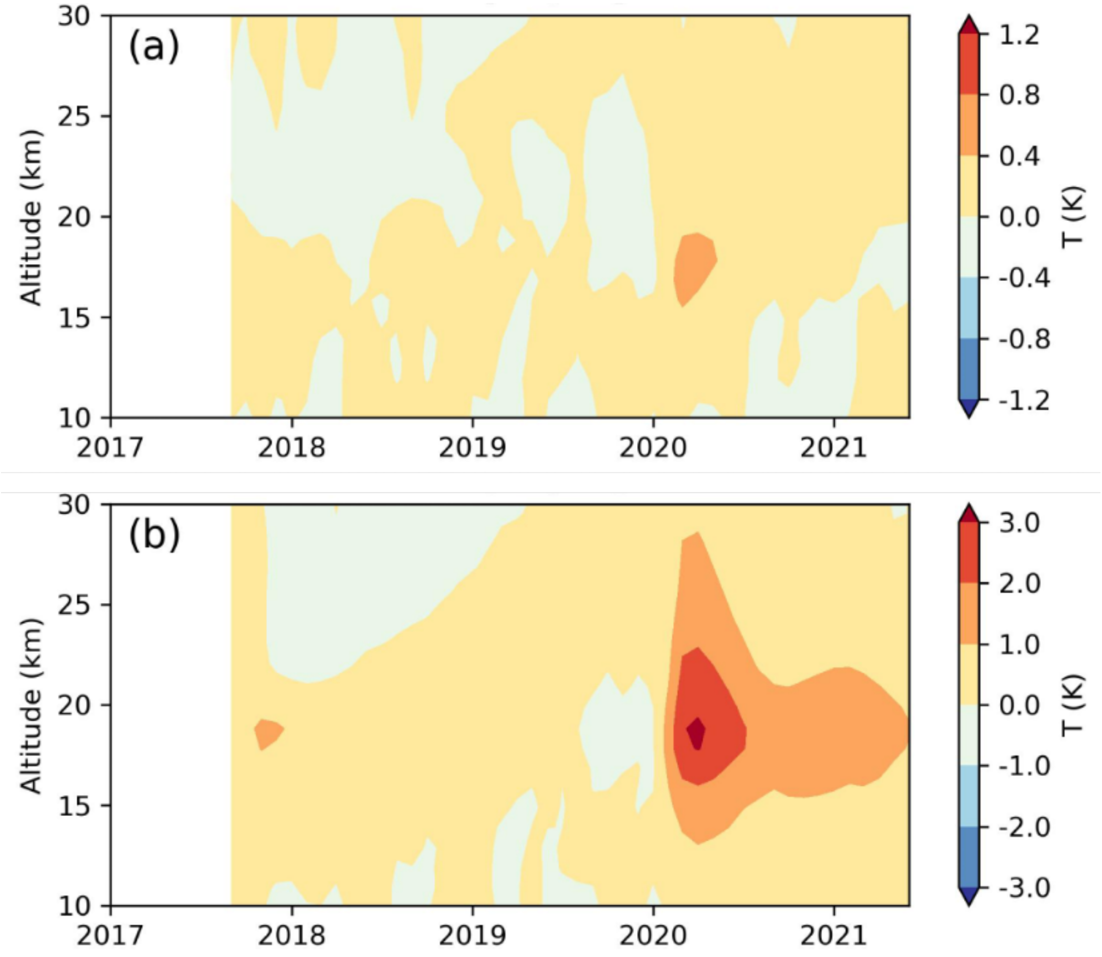

Figure S3. Comparison of stratospheric warming for pyroCb smoke with (a) 0% BC and (b) 10% BC.

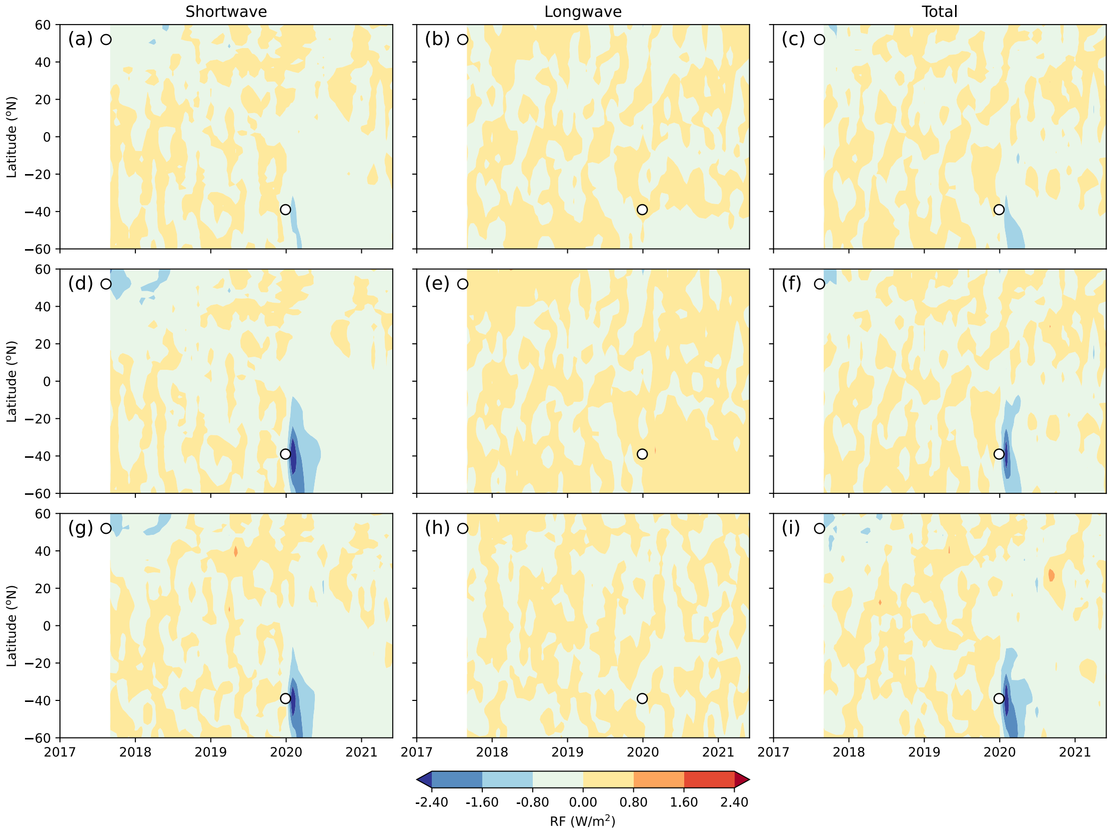

Figure S4. Latitudinal distribution of RF at the TOA (a - c), 200 hPa (d - f), and the surface (g - i). Left to right columns represent shortwave, longwave, and total RF, respectively. The circles represent the injection time and locaitons of PNE and ANY.

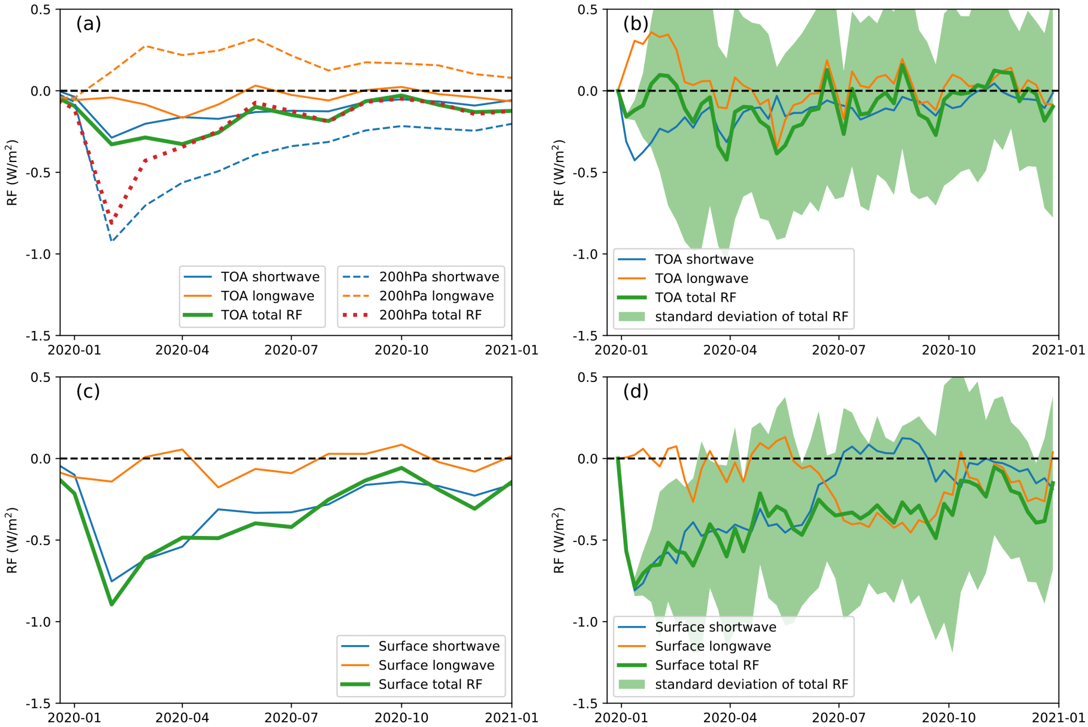

Figure S5. Comparison of RF from MAM3 (left) and CARMA (right). The comparison of RF at the TOA vs. RF at 200 hPa is shown in subplot (a).

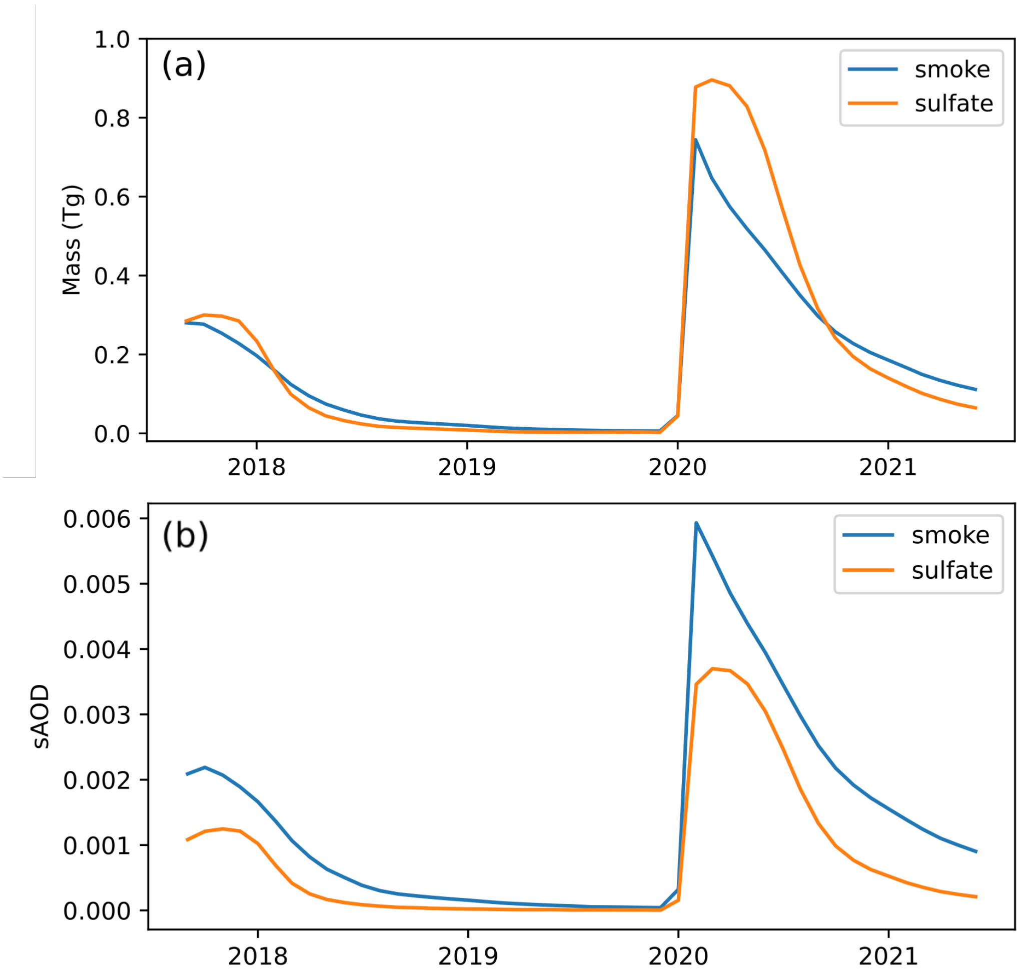

Figure S6. Comparison of pyroCb smoke and volcanic sulfate for (a) global aerosol mass in the stratosphere and (b) global-mean sAOD above 200 hPa. Blue lines indicate smoke and red lines denote sulfate aerosols.

Table S1. Emission Inventory of pyroCb smoke in our model.

PyroCb	Date	Duration (h)	Latitude (ºN)	Longitude (ºE)	Height (km)	Mass (Tg)	BC (%)
2017 PNE	2017 Aug. 12	5	52	-120	12	0.3	2
2019-2020 ANY	2019 Dec. 29	5	-39	150	12	0.9	2.5
	2019 Dec. 30	5					
	2019 Dec. 31	5					
	2020 Jan. 4	5					

Table S2. Refractive Indices at 550 nm used in MAM3 (Bond & Bergstrom, 2006; Hess et al., 1998; Liu et al., 2012) and CARMA (Yu et al., 2015; Yu et al., 2019b).

Aerosol Scheme	RI			Mixing state
	BC	OM	Sulfate	
MAM3	1.95+0.79i	1.53+0.0057i	$1.43+10^{-8}$i	External
CARMA	1.95+0.79i	1.4+0.0i	1.43+0.0i	Internal for BC and External otherwise

Table S3. Aerosol optical properties of BC, OM, and sulfate estimated with the Mie theory. The RI values are from Table S2 for MAM3 at 550 nm wavelength. The aerosol diameter is assumed as 300 nm here. The SSA in the last column refers to single scattering albedo.

MAM3 aerosol	Scattering Efficiency	Backscattering Efficiency	Absorption Efficiency	Extinction Efficiency	SSA
BC (2.5%)	0.0331	0.0009	0.0417	0.0739	0.45
OM (97.5%)	1.2642	0.0461	0.0427	1.3070	0.97
Sulfate	0.8078	0.0364	$6.6746*10^{-8}$	0.8078	1

Table S4. Annual-mean RF values and standard deviation of the means from ensembles. The values were calculated with the global area-weighted mean for 12 months after the 2017 PNE and 2019-2020 ANY pyroCb.

PyroCb	Interface	Shortwave (W/m^2)	Longwave (W/m^2)	Total (W/m^2)
PNE	TOA	-0.05 ± 0.01	0.01 ± 0.02	-0.04 ± 0.02
	200 hPa	-0.12 ± 0.01	0.06 ± 0.02	-0.05 ± 0.02
	Surface	-0.09 ± 0.02	-0.004 ± 0.02	-0.09 ± 0.02
ANY	TOA	-0.13 ± 0.01	-0.04 ± 0.02	-0.17 ± 0.02
	200 hPa	-0.39 ± 0.01	0.17 ± 0.02	-0.22 ± 0.02
	Surface	-0.33 ± 0.02	-0.04 ± 0.02	-0.37 ± 0.03
ANY from Yu et al. 2021	TOA	-0.13 ± 0.01	0.04 ± 0.04	-0.08 ± 0.04
	Surface	-0.23 ± 0.04	-0.14 ± 0.06	-0.37 ± 0.04

Table S5. Comparison of ERF at the TOA between our simulated pyroCb and some significant volcanic ERF reported in the literature. Andersson et al. (2015) estimated three RF values for the Kasatochi, Sarychev, and Nabro eruptions during 2008 Aug. and 2011 Jun. The annual-mean volcanic RF values in 2008, 2009, and 2011 were reported by (Schmidt et al., 2018; Schmidt et al., 2014).

Event	Name	Mass (Tg)	Annual-mean ERF (W/m^2)	Annual-mean ERF per mass ($W\ m^{-2}\ Tg^{-1}$)
pyroCb	PNE	0.3	-0.04	-0.13
	ANY	0.9	-0.17	-0.19
Volcanic eruptions	Kasatochi	1.7	-0.03 to -0.15	-0.02 to -0.09
	Sarychev	1.2	-0.13 to -0.26	-0.11 to -0.22
	Nabro	1.5	-0.11 to -0.15	-0.07 to -0.10

Table S6. Same as Table S4 but for RF from mass-equivalent volcanic sulfate.

Equivalent sulfate	Interface	Shortwave (W/m^2)	Longwave (W/m^2)	Total (W/m^2)
PNE-sulfate (MAM3)	TOA	-0.04 ± 0.01	0.02 ± 0.02	-0.02 ± 0.02
	200 hPa	-0.04 ± 0.01	0.02 ± 0.02	-0.02 ± 0.02
	Surface	-0.06 ± 0.02	0.02 ± 0.02	-0.04 ± 0.03
ANY-sulfate (MAM3)	TOA	-0.13 ± 0.01	0.03 ± 0.02	-0.10 ± 0.02
	200 hPa	-0.13 ± 0.01	0.03 ± 0.01	-0.10± 0.02
	Surface	-0.11 ± 0.02	0.007 ± 0.02	-0.10 ± 0.03
ANY-sulfate (CARMA)	TOA	-0.19 ± 0.02	0.01 ± 0.02	-0.18 ± 0.03
	Surface	-0.11 ± 0.04	-0.09 ± 0.06	-0.20 ± 0.03